

An Enhanced Submodule for Modular Multilevel Converter with DC Fault Ride-Through Capability

Yu Liu, Shengbo Zhang, and Yating Yuan

Abstract—Modular multilevel converter (MMC) has been successfully applied in various power electronic systems owing to its high efficiency, scalability, and superior output performance. Although the half-bridge submodule (HBSM) is widely used in MMCs for its structural simplicity, it is incapable of handling direct-current (DC) short-circuit faults. The diode-clamp submodule (DCSM) addresses this limitation by providing DC fault ride-through capability. However, because its two identical capacitors are connected in series, the equivalent capacitance is halved. To overcome this drawback, an enhanced SM is proposed in this paper. For the same energy storage capacity, the proposed SM reduces the total required capacitance by 75% compared with the DCSM. In addition, the proposed SM requires one fewer diode than the DCSM, thereby lowering the overall MMC capital cost. The topology and the operating modes of the proposed SM are described in detail, and its functionality is experimentally validated. The results demonstrate that the proposed SM can suppress DC fault currents and restore normal operation without additional external protection devices.

Index Terms—Modular multilevel converter (MMC), fault ride-through capability.

I. Introduction

MODULAR multilevel converter (MMC) has been successfully employed in various high-voltage direct current applications such as point-to-point systems [1] or multi-terminal systems [2], [3]. Moreover, it can be employed in flexible alternating current transmission system [4], static compensator [5], motor drives [6], and medium-to low-voltage direct-current (DC) grids [7]. Owing to its high modularity and scalability, high energy efficiency, high voltage rating, low harmonics distortion, and the absence of DC link [8], the technology has attracted considerable research interest. Consequently, numerous topologies and control methods have been proposed in the literature.

In an MMC, the multilevel voltage waveform is generated by switching multiple submodules (SMs) connected in series. The half-bridge submodule (HBSM) is the first submodule topology proposed for MMC [9], and it has been most commonly used [10]. The HBSM contains only one capacitor and two switches, making it cost-effective and easy to control. However, it can only block

current through the lower arm in one direction. Current in the opposite direction flows freely through the free-wheeling diode. Thus, the HBSM lacks the capability to interrupt short-circuit fault currents. To clear fault currents, additional devices such as circuit breakers must be installed on either the alternating current- (AC) or DC-side of the MMC. Notably, a circuit breaker typically requires several cycles to clear a fault, resulting in a slow fault clearance [8].

To endow the MMC with fault-handling capability, the diode-clamp submodule (DCSM) was proposed in [11]. Compared with an HBSM, the DCSM contains one extra switch, one extra capacitor, and two additional diodes. The extra switch is connected in anti-series with the lower-arm switch of the HBSM, enabling it to block current in the reverse direction and thus allowing the lower arm to block current in either direction. The extra capacitor is used to absorb power and provide voltage support when fault current flows in the reverse direction. However, the DCSM contains two identical capacitors connected in series, which reduces the equivalent capacitance to half of the individual capacitance.

Given that an MMC typically consists of hundreds or even thousands of SMs, any additional cost for a single component will result in a significantly higher capital cost for the entire MMC station. To reduce the capital cost of the MMC, an enhanced HBSM is proposed in this paper. Similar to the DCSM, the proposed SM can autonomously suppress DC fault currents and resume normal operation after fault clearance. More importantly, for the same energy storage capacity, the proposed SM requires a smaller total capacitance and one fewer diode than the DCSM, thereby reducing the overall capital cost of the MMC.

This paper is organized as follows: Section II presents the topology and operating modes of the proposed SM. Then, the functionality and the performance of the proposed SM is demonstrated through a physical experiment in section III. Finally, conclusions are drawn in Section IV.

II. Topology and operating modes of the Proposed Submodule

To reduce the component count while maintaining fault-handling capability, a novel topology of an SM is proposed as the circuit diagram shown in Fig. 1. The proposed SM is a two-port circuit network, which consists of three fully controlled switches S_1 – S_3 , three diodes D_1 – D_3 , and

Yu Liu and Shengbo Zhang are with the College of Urban Transportation and Logistics, Shenzhen Technology University, Shenzhen, China.

Yating Yuan is with the Department of Applied Mathematics, University of Waterloo, 200 University Avenue, Waterloo, Ontario, Canada.

Manuscript received June 21, 2026. Corresponding authors: Yu Liu (liuyu@sztu.edu.cn) and Yating Yuan (yating.yuan@uwaterloo.ca).

two capacitors C_1, C_2 where $C_1 > C_2$. The switches and diodes form a half-bridge configuration: the upper arm comprises switch S_1 with an anti-parallel connected diode D_1 , while the lower arm consists of switches S_2 and S_3 connected in anti-series, each with an anti-parallel diode. The corresponding diodes in the lower arm are thus also in anti-series. The diodes serve to clamp the voltages across the switches and provide a free-wheeling path for current when the switches are turned off. Capacitor C_1 is connected in parallel to the branch formed by S_1 and S_2 , while capacitor C_2 is connected in parallel with the entire half-bridge. Compared with a DCSM [11], a proposed SM requires one fewer diode, thereby reducing the component count and overall system complexity for the MMC.

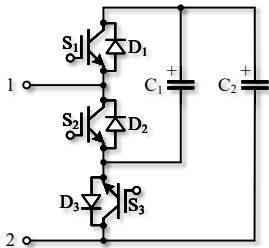


Fig. 1. Circuit topology of the proposed SM.

The proposed SM features three operating modes similar to those of the conventional HBSM, namely, the inserted mode, the bypassed mode, and the blocked mode. During normal operation, the SM switches between the inserted and bypassed modes. Moreover, existing control methods suitable for the HBSM can also be directly applied to the proposed SM.

A. Mode 1: Inserted Mode

In this mode, S_1 and S_3 are turned on, whereas S_2 is turned off. Consequently, the upper arm conducts while the lower arm is blocked, and both capacitors are connected in parallel and inserted into the external circuit. The current path in the SM is marked in orange, as shown in Fig. 2(a). When current enters the SM at port 1 ($i_{SM} > 0$), it flows through diode D_1 and then splits into two branches: one branch goes through C_1 and D_3 , while the other flows through C_2 . Finally, the two branches merge at port 2. During this process, the capacitors are charging, and their voltages v_{c1} and v_{c2} increase.

Conversely, when current enters the SM from port 2 ($i_{SM} < 0$), it also splits into two branches: one flows through S_3 and C_1 , while the other flows through C_2 . Both paths then merge and flow through S_1 to port 1. In this case, the capacitors are discharging, and v_{c1} and v_{c2} decrease. The voltage across the two ports, v_{SM} , can be calculated as follows:

$$v_{SM} = \begin{cases} v_{c1} + v_{d1} + v_{d3} = v_{c2} + v_{d1}, & \text{if } i_{SM} > 0 \\ v_{c1} + v_{s1} + v_{s3} = v_{c2} + v_{s1}, & \text{if } i_{SM} < 0 \end{cases}, \quad (1)$$

where v_{s1} , v_{s3} , v_{d1} , and v_{d3} are the voltage drops across S_1 , S_3 , D_1 , and D_3 , respectively. During normal operation, these voltage drops are much smaller than the capacitor voltages, yielding $v_{SM} \approx v_{c1} \approx v_{c2}$ in this mode. Therefore, the two capacitors are effectively connected in parallel regardless of the direction of i_{SM} .

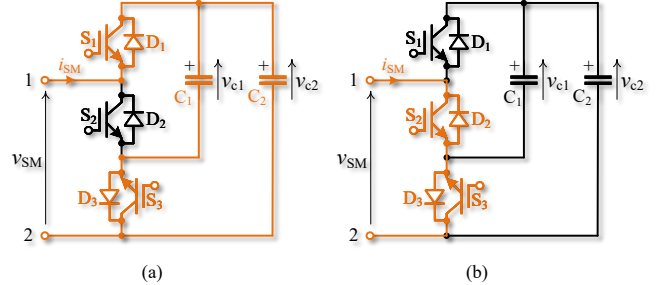


Fig. 2. Current path in the SM during normal operation: (a) inserted mode; (b) bypassed mode.

B. Mode 2: Bypassed Mode

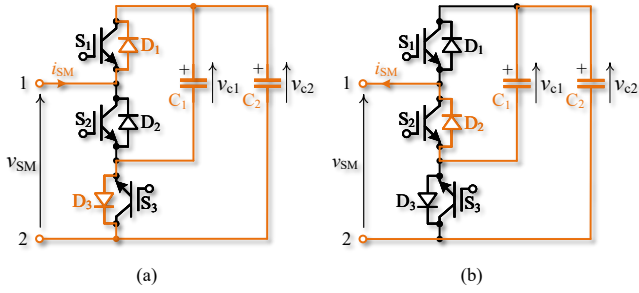
When S_1 is turned off and S_2 and S_3 are turned on, the upper arm is blocked while the lower arm conducts, and the SM operates in the bypassed mode. The current path is shown in orange in Fig. 2(b). When $i_{SM} > 0$, it flows directly through S_2 and D_3 , and then exits the SM through port 2. When $i_{SM} < 0$, it flows through S_3 and D_2 , and then exits the SM through port 1. In both cases, i_{SM} does not flow through the capacitors. Hence, the capacitors are bypassed and their voltages remain constant, neglecting losses. In this mode, C_1 and C_2 are always connected in parallel regardless of the direction of i_{SM} , and v_{SM} can be calculated as follows:

$$v_{SM} = v_{s2} + v_{d3} = v_{s3} + v_{d2} \approx 0. \quad (2)$$

In Modes 1 and 2, C_1 and C_2 are connected in parallel, yielding an equivalent capacitance of $C_{eq,p} = C_1 + C_2$, which is greater than C_1 . Moreover, C_2 is designed such that $C_2 \ll C_1$. By contrast, the two capacitors in the DCSM are connected in series and are identical [11], i.e., $C_1 = C_2$, resulting in an equivalent capacitance of $C_{eq,d} = \frac{1}{2}C_1$. Therefore, for the same individual capacitors, $C_{eq,p} > C_{eq,d}$, indicating that the proposed SM offers greater energy storage capability than the DCSM. Equivalently, to achieve the same equivalent capacitance, the proposed SM requires only 25% of the total capacitance required by the DCSM, thereby reducing the capacitor cost in the MMC.

C. Mode 3: Blocked Mode

When all switches S_1 – S_3 are turned off, the SM operates in the blocked mode. This mode can be adopted during the startup process to charge the capacitor voltages to the preset value, or when a short-circuit fault occurs. When $i_{SM} > 0$, the current flows through D_1 and then splits into two branches: one flows through C_1 and D_3 , while the


 Fig. 3. Current path in the blocked mode: (a) $i_{SM} > 0$; (b) $i_{SM} < 0$.

other flows through C_2 . Finally, the two branches merge at port 2. The current path is shown in orange in Fig. 3(a). In this case, the two capacitors are connected in parallel, and v_{SM} can be calculated as eq. (1). If i_{SM} is a fault current, it will be suppressed because the boosting direction of v_{SM} opposes the direction of i_{SM} in this mode.

If $i_{SM} < 0$, however, the current flows successively through C_2 , C_1 , and then D_2 to port 1. The current path through the SM is shown in Fig. 3(b). Unlike the previous case, C_1 and C_2 are connected in series in this mode, with v_{c1} increasing while v_{c2} decreases. The voltage v_{SM} can then be calculated as follows:

$$v_{SM} = v_{c2} - v_{c1} - v_{d2}. \quad (3)$$

In Modes 1 and 2, $v_{c1} \approx v_{c2}$. Thus, v_{SM} is initially zero when the SM transitions from either of these modes to Mode 3. Once blocked, v_{c2} decreases while v_{c1} increases because the two capacitors are connected in anti-series, resulting in a negative v_{SM} that continuously decreases. Since $C_1 > C_2$, v_{c2} decreases at a higher rate than v_{c1} increases. Consequently, v_{SM} becomes increasingly negative, establishing a voltage that opposes i_{SM} and thereby suppresses the fault current.

III. Experimental Verification

The proposed SM topology is verified through an experiment in which the SM is applied to a three-phase MMC that can operate either as an inverter or a rectifier. The circuit topology of the MMC is depicted in Fig. 4, the experimental setup is shown in Fig. 5, and the system parameters are listed in Table I. The main circuit is constructed using discrete components. The nearest level control algorithm [12] is adopted and implemented by an RTU-BOX206 controller from RTUnit to regulate the converter.

TABLE I

Parameters used in the experiment.

Parameter	Value	Parameter	Value
C_1 (μF)	470	C_2 (μF)	47
L_{arm} (mH)	1	R_{load} (Ω)	10
$v_{s,dc}$ (V)	10	$v_{s,abc}$ (ph-ph, RMS, V)	6.12

When the MMC operates in inverter mode, its DC side is powered by a DC voltage source with an output voltage

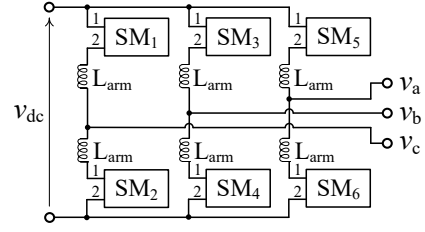


Fig. 4. Circuit diagram of the MMC in the experiment.

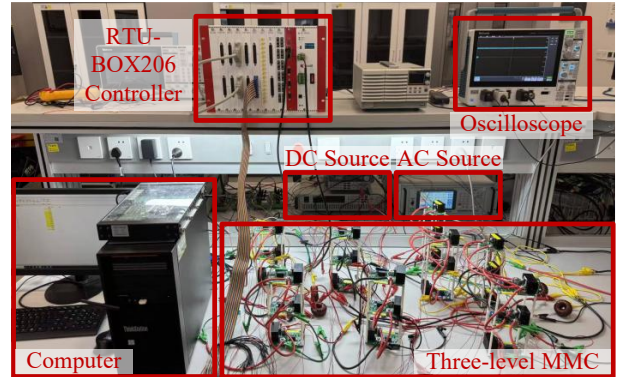


Fig. 5. Experimental setup for the verification.

of $v_{s,dc}$, and is connected to two resistors R_{load} connected in series. The waveforms of the output voltages on the AC side are plotted in Fig. 6(a). As can be observed from Fig. 6(a), the MMC can invert the DC voltage into a 50 Hz three-phase three-level AC voltage using the proposed SM topology.

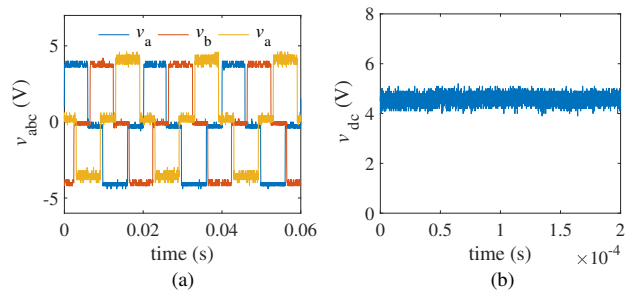


Fig. 6. Output voltages of the MMC in normal operations: (a) AC voltages in the inverter mode; (b) DC voltage in the rectifier mode.

Conversely, when the MMC operates in rectifier mode, its AC terminals are fed by a three-phase voltage source with phase voltages $v_{s,abc}$. Each phase is connected to a resistive load R_{load} . The DC-side output voltage waveform is shown in Fig. 6(b). As observed in Fig. 6(b), using the proposed SM topology, the MMC can operate as a rectifier and produce a stable DC voltage. Furthermore, the two capacitor voltages remain approximately equal to each other, as shown in Fig. 7.

During rectification, a DC-side short-circuit fault is applied at approximately $t = 2.7$ s. As shown in Fig. 8(a), the arm-current amplitudes of the MMC increase rapidly.

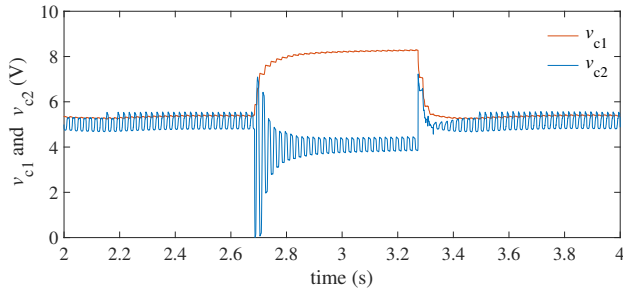


Fig. 7. Voltage response of the capacitors in SM₁ during DC fault.

Once the current exceeds a preset threshold value I_{arm}^{th} , which is set to -0.3 A in the experiment, the SMs enter Mode 3 by turning off all IGBTs. Consequently, both capacitors in each SM are inserted into the external circuit, as illustrated in Fig. 3.

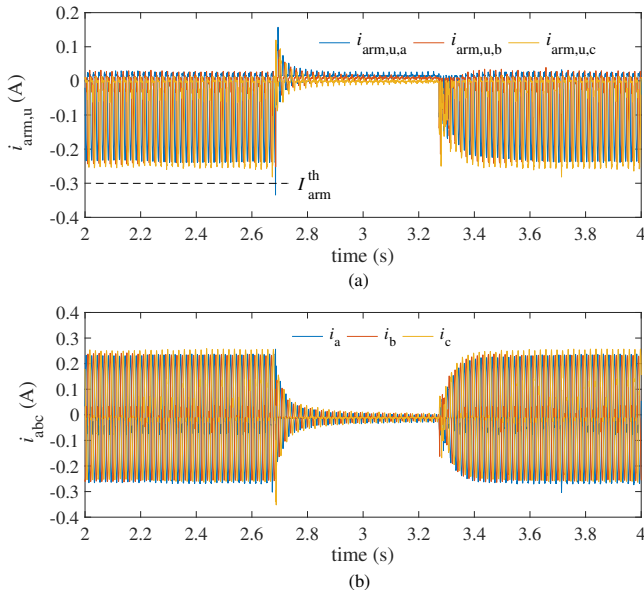


Fig. 8. Current response of the MMC during DC fault: (a) upper arm currents; (b) AC-side currents.

During rectifier operation, $v_{c1} \approx v_{c2}$, and i_{SM} is predominantly negative, as can be observed from Fig. 7 and Fig. 8(a), respectively. Therefore, once the SM is blocked, v_{c2} decreases while v_{c1} increases, as illustrated by the capacitor voltages of SM₁ in Fig. 7. Because the two capacitors are connected in anti-series, the voltage across the SM becomes increasingly negative and opposes the fault current, forcing the arm currents to decay, as shown in Fig. 8(a). Consequently, the AC-side currents of the MMC are also reduced, as depicted in Fig. 8(b).

At approximately $t = 3.3$ s, the DC fault is cleared and all SMs revert to Mode 1 or Mode 2. The arm currents, AC-side currents, and capacitor voltages automatically return to their pre-fault levels, as shown in Fig. 7 and Fig. 8. This confirms that the proposed SM topology can ride through DC short-circuit faults without external protection devices.

IV. Conclusion

This paper has presented an enhanced HBSM with DC fault ride-through capability for MMCs. The topology and operating modes of the proposed SM are described in detail, and its performance is experimentally validated. Similar to the DCSM, the proposed SM can autonomously suppress fault currents and resume normal operation after fault clearance without relying on additional external protection devices. Unlike the DCSM, however, the proposed SM requires a smaller total capacitance while offering greater energy storage capability, and each proposed SM uses one fewer diode than the DCSM. These advantages help reduce the system complexity and overall capital cost of the MMC.

References

- [1] Y. Yuefeng, Y. Jie, H. Zhiyuan, and W. Haitian, "Research on control and protection system for Shanghai Nanhai MMC VSC-HVDC demonstration project," in 10th IET International Conference on AC and DC Power Transmission (ACDC 2012), Dec. 2012, pp. 1–6. [Online]. Available: <https://ieeexplore.ieee.org/document/6521268/>
- [2] X. Li, Z. Yuan, J. Fu, Y. Wang, T. Liu, and Z. Zhu, "Nanao multi-terminal VSC-HVDC project for integrating large-scale wind generation," in 2014 IEEE PES General Meeting | Conference & Exposition, Jul. 2014, pp. 1–5, ISSN: 1932-5517. [Online]. Available: <https://ieeexplore.ieee.org/document/6939123/>
- [3] G. Tang, H. Pang, and X. Wei, "Research on Key Technology and Equipment for Zhangbei 500kV DC Grid," in 2018 International Power Electronics Conference (IPEC-Niigata 2018 -ECCCE Asia), May 2018, pp. 2343–2351. [Online]. Available: <https://ieeexplore.ieee.org/document/8507575/>
- [4] P. Sotoodeh and R. D. Miller, "Design and Implementation of an 11-Level Inverter With FACTS Capability for Distributed Energy Systems," IEEE Journal of Emerging and Selected Topics in Power Electronics, vol. 2, no. 1, pp. 87–96, Mar. 2014. [Online]. Available: <https://ieeexplore.ieee.org/document/6677533/>
- [5] X. Yu, Y. Wei, and Q. Jiang, "STATCOM Operation Scheme of the CDSM-MMC During a Pole-to-Pole DC Fault," IEEE Transactions on Power Delivery, vol. 31, no. 3, pp. 1150–1159, Jun. 2016. [Online]. Available: <https://ieeexplore.ieee.org/document/7177121/>
- [6] R. Picas, J. Zaragoza, J. Pou, S. Ceballos, G. Konstantinou, and G. J. Capella, "Study and Comparison of Discontinuous Modulation for Modular Multilevel Converters in Motor Drive Applications," IEEE Transactions on Industrial Electronics, vol. 66, no. 3, pp. 2376–2386, Mar. 2019. [Online]. Available: <https://ieeexplore.ieee.org/document/8396868>
- [7] S. Zhao, Y. Chen, S. Cui, B. J. Mortimer, and R. W. De Doncker, "Three-Port Bidirectional Operation Scheme of Modular-Multilevel DC–DC Converters Interconnecting MVDC and LVDC Grids," IEEE Transactions on Power Electronics, vol. 36, no. 7, pp. 7342–7348, Jul. 2021. [Online]. Available: <https://ieeexplore.ieee.org/document/9275393/>
- [8] S. Debnath, J. Qin, B. Bahrani, M. Saeedifard, and P. Barbosa, "Operation, Control, and Applications of the Modular Multilevel Converter: A Review," IEEE Transactions on Power Electronics, vol. 30, no. 1, pp. 37–53, Jan. 2015. [Online]. Available: <https://ieeexplore.ieee.org/document/6757006>
- [9] A. Lesnicar and R. Marquardt, "An innovative modular multilevel converter topology suitable for a wide power range," in 2003 IEEE Bologna Power Tech Conference Proceedings, vol. 3, Jun. 2003, pp. 6 pp. Vol.3–. [Online]. Available: <https://ieeexplore.ieee.org/document/1304403/>
- [10] J. D. Páez, D. Frey, J. Maneiro, S. Bacha, and P. Dworakowski, "Overview of DC–DC Converters Dedicated to HVdc Grids," IEEE Transactions on Power Delivery, vol. 34, no. 1, pp. 119–128, Feb. 2019. [Online]. Available: <https://ieeexplore.ieee.org/document/8379435/>

- [11] X. Li, W. Liu, Q. Song, H. Rao, and S. Xu, "An enhanced MMC topology with DC fault ride-through capability," in IECON 2013 - 39th Annual Conference of the IEEE Industrial Electronics Society, Nov. 2013, pp. 6182–6188, iSSN: 1553-572X. [Online]. Available: <https://ieeexplore.ieee.org/document/6700152/>
- [12] Q. Tu and Z. Xu, "Impact of Sampling Frequency on Harmonic Distortion for Modular Multilevel Converter," IEEE Transactions on Power Delivery, vol. 26, no. 1, pp. 298–306, Jan. 2011. [Online]. Available: <https://ieeexplore.ieee.org/document/5673482/>